Journal of Controlled Release 365 (2024) 969–980

Contents lists available at ScienceDirect

Journal of Controlled Release

journal homepage: www.elsevier.com/locate/jconrel

A cell-free, biomimetic hydrogel based on probiotic membrane vesicles ameliorates wound healing

Thomas Kuhn [a,b,1], Ahmad Aljohmani [c,1], Nicolas Frank [a,b], Lina Zielke [a], Mina Mehanny [a,d], Matthias W. Laschke [e], Marcus Koch [f], Jessica Hoppstädter [b], Alexandra K. Kiemer [b], Daniela Yildiz [c,*], Gregor Fuhrmann [a,b,g,h,*]

[a] Helmholtz Institute for Pharmaceutical Research Saarland (HIPS), Helmholtz Centre for Infection Research (HZI), Campus E8.1, Saarbrücken 66123, Germany
[b] Department of Pharmacy, Saarland University, Campus E8.1, 66123 Saarbrücken, Germany
[c] Institute of Experimental and Clinical Pharmacology and Toxicology, PZMS, Saarland University, 66421 Homburg, Germany
[d] Department of Pharmaceutics and Industrial Pharmacy, Faculty of Pharmacy, Ain Shams University, 11566 Cairo, Egypt
[e] Institute for Clinical and Experimental Surgery, Saarland University, Homburg, Germany
[f] INM – Leibniz Institute for New Materials, Campus D2 2, 66123, Saarbrücken, Germany
[g] Friedrich-Alexander-Universität Erlangen-Nürnberg, Department of Biology, Pharmaceutical Biology, Staudtstr. 5, 91058 Erlangen, Germany
[h] FAU NeW – Research Center New Bioactive Compounds, Nikolaus-Fiebiger-Str. 10, 91058 Erlangen, Germany

ARTICLE INFO

Keywords:
Bacteriomimetics
Probiotic bacteria
Lactobacilli
Bacterial membrane vesicles
Extracellular vesicles
Inflammation
Wound healing

ABSTRACT

Probiotic bacteria, such as *Lactobacilli,* have been shown to elicit beneficial effects in various tissue regeneration applications. However, their formulation as living bacteria is challenging, and their therapeutic use as proliferating microorganisms is especially limited in immunocompromised patients.

Here, we propose a new therapeutic avenue to circumvent these shortcomings by developing a bacteriomimetic hydrogel based on membrane vesicles (MVs) produced by *Lactobacilli*. We coupled MVs from *Lactobacillus plantarum* and *Lactobacillus casei*, respectively, to the surface of synthetic microparticles, and embedded those bacteriomimetics into a pharmaceutically applicable hydrogel matrix. The wound microenvironment changes during the wound healing process, including adaptions of the pH and changes of the oxygen supply. We thus performed proteomic characterization of the MVs harvested under different culture conditions and identified characteristic proteins related to the biological effect of the probiotics in every culture state. In addition, we highlight a number of unique proteins expressed and sorted into the MVs for every culture condition. Using different *in vitro* models, we demonstrated that increased cell migration and anti-inflammatory effects of the bacteriomimetic microparticles were dependent on the culture condition of the secreting bacteria. Finally, we demonstrated the bacteriomimetic hydrogel's ability to improve healing in an *in vivo* mouse full-thickness wound model. Our results create a solid basis for the future application of probiotic-derived vesicles in the treatment of inflammatory dispositions and stimulates the initiation of further preclinical trials.

1. Introduction

Skin is the largest organ of the human body and the one that is most exposed to environmental influences and exogenous noxae, such as pathogens, toxins and physical trauma [1,2].Healing of wounds caused by such traumata is a complex interplay of various cells and mediators. Typically, wound healing occurs in three phases consisting of an inflammatory phase, a proliferative phase and a remodeling phase resulting in a mature scar and recovery of the injured tissue [3,4]. However, an overshooting inflammatory reaction may impair wound healing, leading to delayed wound closure, chronic wounds, and the formation of hypertrophic scars [5,6]. Wound healing disorders pose a substantial burden on healthcare systems worldwide, with more than eight million patients and treatment costs of >25 billion $ in the US alone [7,8]. However, current therapy guidelines do not address overshooting inflammation as a main contributor to wound healing disorders, but focus mostly on wound cleaning and management of the wound milieu [9]. Moreover, there has been numerous evidence of scar

* Corresponding authors.
E-mail addresses: daniela.yildiz@uks.eu (D. Yildiz), gregor.fuhrmann@helmholtz-hips.de, gregor.fuhrmann@fau.de (G. Fuhrmann).
[1] First authors with equal contributions

https://doi.org/10.1016/j.jconrel.2023.12.011
Received 31 March 2023; Received in revised form 21 November 2023; Accepted 4 December 2023
Available online 19 December 2023

less, inflammation-free wound healing that was observed in the healing of fetal wounds. These observations support the hypothesis that modulating overshooting immune reactions may also lead to an improved healing process. This highlights the potential of targeting the immune reaction with suitable therapeutics to augment wound healing [10,11].

A novel therapeutic route is the use of probiotic bacteria [12,13]. These have been shown to elicit multiple biological effects in the context of wound healing, including antimicrobial effects against pathogenic bacteria in the wound, interactions with the host inflammatory response, as well as pH alteration of the wound milieu [13]. However, safety and applicability concerns have been raised regarding the use of live, proliferative bacteria as therapeutics, especially in the context of immunocompromised patients [14].

A promising alternative might be the use of probiotic bacterial membrane vesicles (MVs) as explored in the recent studies. Bacterial MVs are a class of biogenic nanoparticles shed by almost every microorganism. [15,16] They are characterized by a diameter of 50–150 nm and are composed of a phospholipid membrane, as well as multiple types of cargoes [17]. Possible cargoes include a variety of nucleic acids and proteins. They have been shown to fulfill many biological roles in cell-cell communication, in particular in the communication of bacteria and their host immune system, exerting similar biological effects to those of the live bacteria [18]. One example are the Gram-positive *Lactobacillus (L.)* strains L. *casei* and *L. plantarum*, which possess immune-regulating properties [19–21]. Their potential to induce the regulatory M2 phenotype in macrophages makes them interesting candidates for the treatment of poorly healing wounds [22].

Therefore, in our recent study, we assessed a hydrogel containing bacteriomimetic microparticles as alternative to augment wound healing. These bacteriomimetics are a biomimetic therapeutic system composed of MVs derived from probiotic *Lactobacilli* coupled onto synthetic microparticles. We formulated the bacteriomimetics in a pharmaceutical hydrogel for better applicability and as a cutaneous therapeutic option for wound healing disorders [23,24]. Probiotic and commensal bacteria are physiologically relevant in wound healing but different pH and oxygen-supply conditions that occur during wound healing, may overall influence their biological activity [25]. To optimize the biological effect of the MVs used, we mimicked such conditions during bacterial culture and investigated their effect on the MVs' biological effects (Fig. 1). We evaluated the anti-inflammatory effect of the bacteriomimetics on primary human peripheral blood mononuclear cells and further demonstrated their ability to reduce scar formation in a

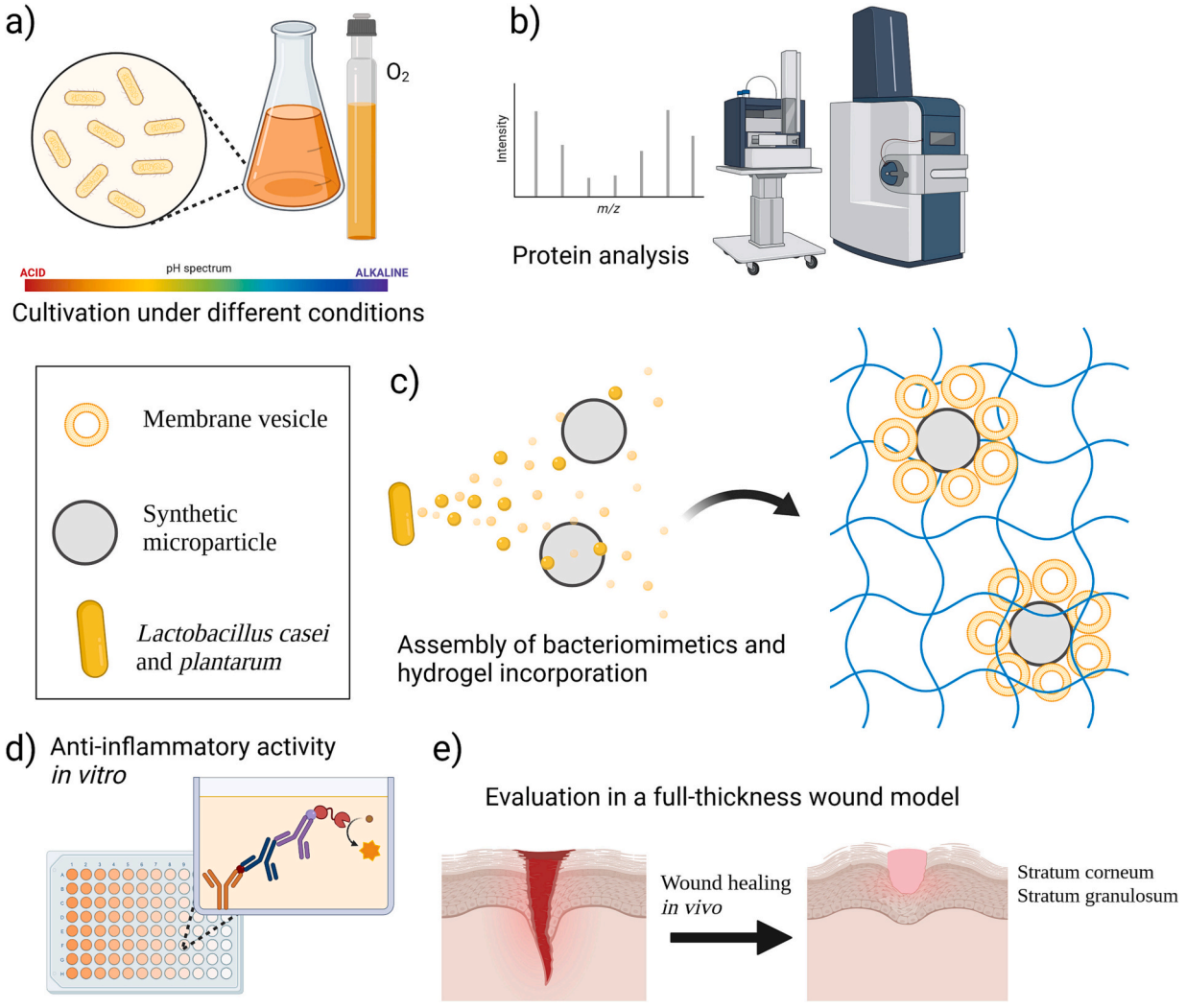

Fig. 1. Schematic overview of the present study. (a) Lactobacillus strains *L. plantarum* and *L. casei* were cultivated under various culture conditions, including different media pH-values and oxygen supply. (b) The cargo proteins within and on the surface of the MVs were characterized using LC-MS. (c) The harvested membrane vesicles were coupled to synthetic microparticles, creating a bacteriomimetic therapeutic system, which could then be formulated in a skin-applicable hydrogel. (d) The anti-inflammatory activity and their potential to improve wound healing and reduce scarring were studied in different *in vitro* models (determination of their influence on cytokine production *via* ELISA, as well as cell migration *via* keratinocyte scratch assays) and (e) in a mouse model. The figure was made using BioRender software. LC-MS, liquid chromatography–mass spectrometry; MV, membrane vesicles.

mouse *in vivo* model. In our study, we combined the inherent positive effects on wound healing of both hydrogels and our bacteriomimetic microparticles. With our easy-to-prepare hydrogel loaded with bacteriomimetic microparticles, we underline the potential of using bacterial MVs as a therapeutic avenue for wound healing disorders.

2. Results and discussion

2.1. Proteomic characterization of the purified MVs

We cultured the *Lactobacilli* in various culture conditions resembling the conditions in the human intestine where the living bacteria's probiotic effects were first proven [26] to further characterize their MVs. Supplementary Fig. S1 shows size profiles and MV yield in comparison to media controls, and purification profiles of MVs by size exclusion chromatography. The morphology of the vesicles was verified by cryoelectron microscopy (Supplementary Fig. S2). To specify the composition and the cargos of the MVs, mass spectrometry analysis was performed. The unique proteins found with the highest coverage for every culture condition are listed in the Supplementary Table S1, and a full list of proteins is found in the Supplementary List (all proteins).

For both strains, a high number of proteins, namely 125 for *L. casei* and 101 for *L. plantarum* were present in all conditions (Fig. 2). For *L. casei,* all samples showed an abundance of p40 and p75 muramidases, which have been described as contributors to the probiotic, effect of the live bacteria before [27,28]. The *L. casei* pH 5 cultures showed an abundance of universal stress proteins, indicating a preference for higher pH-values, which was also highlighted for MVs harvested from this culture condition [29]. *L. casei* pH 6.5 cultures presented the identification of thioredoxin, a protein associated with response to oxidative stress, which was neither abundant in the anaerobic culture nor the pH 5 and pH 8 cultures [30]. In contrast, in the pH 8 cultures of *L. casei* we identified various enzymes involved in nucleotide metabolism, such as S-adenosylmethionine:tRNA ribosyltransferase-isomerase and Proline-tRNA ligase. Interestingly, these proteins are typically present in the cytoplasm. These findings were in contrast to the proteins identified at pH 5, pH 6.5, and anaerobic cultures, where more proteins linked to the cell wall and the bacterial membrane were detected.

In *L. plantarum,* common cell surface proteins were found in all culture conditions included hydrolases such as autolysin Acm2, and metabolic enzymes such as Glyceraldehyde-3-phosphate dehydrogenase [31]. Overall, the MV proteins from *L. plantarum* differed strongly in relation to the culture condition applied. In the pH 5, pH 6.5, and anaerobic cultures, mostly extracellular and cell-wall related proteins occurred, such as hydrolases and ion transporters. Interestingly, pH 8 cultures showed a considerably higher abundance of intracellular, metabolism-related proteins, as well as ribosome components. This higher abundance of intracellular proteins in both strains could indicate a different and more random process of MV biogenesis at higher pH medium, like bubbling cell death, whereas the high abundance of cell-wall degrading enzymes could indicate active MV secretion in the other culture conditions [15,32]. We could also demonstrate in both strains the overlap of the proteins found to be highest for pH 6.5 culture and the anaerobic culture, whereas the number of unique proteins was highest in pH 8 cultures. We thus concluded that medium pH has a stronger influence on the protein content of the resulting MVs than the deprivation of oxygen.

These results are in line with previous findings that culture conditions have a strong impact on the physicochemical properties of the MVs produced by the bacteria [29]. Overall, our proteomic analyses showed presence of common proteins, such as the p40 and p75 muramidases, across all MV samples but also high abundance of unique proteins

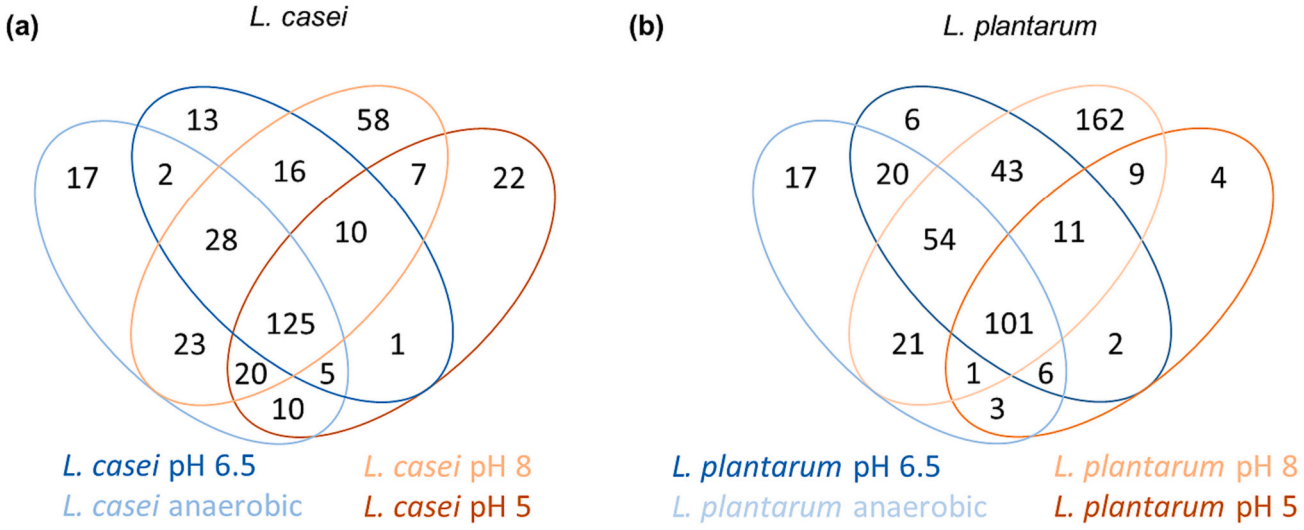

(c)

Protein	Function
p40 cell wall hydrolase	peptidoglycan hydrolase, mucosa-binding[36]
p75 cell wall hydrolase	peptidoglycan hydrolase, cell separation[37]

(d)

Protein	Function
p60 muropeptidase	control of cell length and cell division[38]
glyceraldehyde 3-phosphate dehydrogenase (GAPDH)	extracellular matrix binding[39]

Fig. 2. Proteomic characterization of the Lactobacillus MVs harvested under different culture conditions. (a) *L. casei* and (b) *L. plantarum*. Venn plots show the overlap of the detected proteins and the number of unique proteins for every culture condition. For both strains, a high number of unique proteins could be found for the pH 8 cultures. (c) Common proteins include p40 and p75 cell wall hydrolases and peptidases for L. *casei* and p60 muropeptidase for L. *plantarum*. *L. plantarum* samples showed mainly extracellular proteins and proteins involved in cell wall remodeling. Each condition was measured in biological triplicates and technical replicates.

depending on the bacterial culture conditions.

2.2. Assembly and characterization of the bacteriomimetics

As mentioned above, the therapeutic use of living bacteria is limited, especially in immunocompromised patients. Therefore, we followed a bacteriomimetic approach to investigate the functional impact of the different protein compositions of MVs. To obtain bacteriomimetics, MVs were purified by ultracentrifugation and size-exclusion chromatography, and coupled to the surface of the commercially available beads with reactive aldehyde groups on their surface creating bacteriomimetic microparticles, BP [23]. We used beads with a size of 3.7 μm, which is within the typical size range of bacteria mimicking direct bacterial interaction. MVs were functionalized to the microparticle surfaces in a simple one-pot reaction, utilizing the reaction between aldehyde groups on the microparticles and lysine residues on proteins abundant on the MV surface [23].

Subsequently, aimed to assess the amount of MVs bound to the microparticle surface. We measured the concentration of proteins in the purified MVs and in the supernatant after the coupling reaction, and quantified thereby the microparticle coverage using Eq. (1) from the method section (Fig. 3a). Interestingly, the lowest surface coverage of 3 and 4% was seen for the MVs harvested from L. *casei* under the standard culture conditions in medium with pH 6.5 and anaerobic conditions, respectively. However, MVs harvested from pH 5 and pH 8 cultures showed a higher particle coverage of 34% and 18%, respectively. While no differences were observed at pH 5 (*L. plantarum* 38%), a tendency towards higher coverage was observed for *L. plantarum* than for *L. casei.* The lowest coverage for *L. plantarum* MVs was observed for anaerobic cultures (14%).

These variations can be partially explained by the differences in protein concentration per single MV (Fig. 3b). Here, we observed that *L. plantarum* pH 5 and pH 6.5 cultures had the highest protein content per particle. These were also the conditions that yielded the highest particle coverage. A similar trend was visible for the *L. casei* pH 5 culture MVs, which yielded both the highest protein amount per particle as well as the highest particle coverage out of all *L. casei* samples. Interestingly, *L. casei* pH 8 did not follow the same trend. MVs harvested from this culture condition showed a high degree of coupling to the microparticles while also containing the lowest amount of protein per MV. In this case, the fraction of membrane-bound proteins as well as the number of free lysine residues may contribute to overall coupling efficiency because similar studies showed the extent of surface modification of model liposomes was proportional to the amount of reactive groups on the surface [33].

The obtained BP were additionally characterized regarding the MVs morphology by scanning electron microscopy and depending on the culture conditions used for the production of the MVs. MVs harvested from anaerobic cultures and the pH 6.5 cultures of both strains were visible as single MVs on the microparticle surface. MVs obtained under pH 5 and pH 8 culture conditions resulted in a uniform coverage of the surface where individual MVs cannot be distinguished (Fig. 3c-d). Having established the microparticle coverage as a reliable in-process control in the manufacturing of the BPs, we subsequently were interested in the biological activity as function of the different protein concentration of the bacteriomimetics.

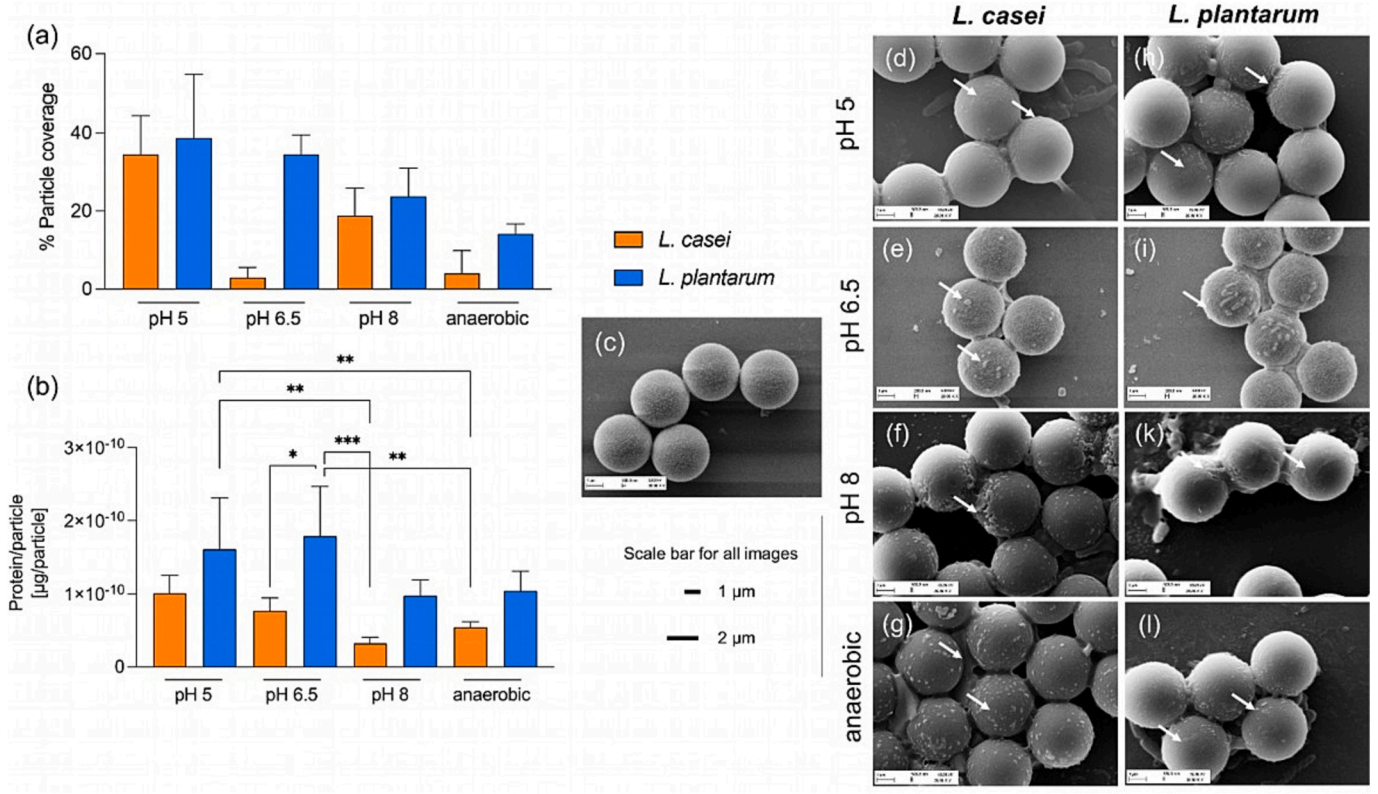

Fig. 3. Characterization of the bacteriomimetic hydrogels. (a) Particle coverage calculated through protein quantification of biomimetics and (b) average protein content per MV for the different culture conditions were determined by bicinchoninic acid assay. In b, the protein content of bulk MVs was normalized to the particle concentration determined by nanoparticle tracking analysis. (c) Untreated beads without MVs and beads coated with MVs (BP) harvested under the different culture conditions and from (d-g) *L. casei* and (h-l) *L. plantarum* as indicated were subjected to scanning electron microscopy. Quantitative data are shown as means + SD calculated from three independent experiments. Statistical differences were analyzed by one-way ANOVA and Tukey's post-hoc test. *$p < 0.05$, **$p < 0.01$, *$p < 0.001$. In addition for data in b), a two-way ANOVA analysis was performed (Supplementary Fig. S3).

2.3. In vitro biocompatibility of MVs and bacteriomimetic microparticles (BP)

First, we tested whether *Lactobacillus* MVs are tolerated by different cell lines to exclude possible cytotoxic effects during wound healing. We used keratinocyte-like HaCaT cells and monocyte-like THP-1 cells as model for skin and immune cells. The THP-1 cells were differentiated into a macrophage-like phenotype using phorbol-12-myristate-13-acetate. As shown in Supplementary Fig. S4, the MVs influenced cell viability only at very high concentrations and for few conditions with high standard deviation. Cytotoxicity in HaCat cells was always below 15% and absent in THP-1 cells, making MVs suitable for further experiments on their biological effects.

During wound healing, cell migration - the process of cells actively moving into the wound site - is physiologically relevant. This process is characterized by a sequence of cellular extension, attachment, contraction and detachment, and is prone to inhibition by the secretome of various bacteria [34,35]. In some models, bacterial treatment was shown to improve the capability of cells to migrate into wounded sites [36,37]. However, for biocompatibility at least no negative effect on migration is essential to avoid inhibition of wound closure. Therefore, we examined the effects of our *Lactobacillus* MVs and the BPs on keratinocyte cell migration using a scratch assay as *in vitro* wound healing model as straightforward technique to study cell migration in real-time. The scratch closure might not only occur upon migration, but also through proliferation of non-migrating cells. However, this was ruled out by mitomycin pretreatment. Extracellular vesicles from mesenchymal stem cells served as a positive control [38,39]. We observed only minor changes compared to an untreated control; all changes in wound closure were found to differ by <10%. Overall, no significant effect on *in vitro* wound closure was observed. (Fig. 3a,b), which in our hands rules out any overshooting cell migration or strong inhibition of cell migration that could lead to insufficient wound closure in an *in vivo* setting. Interestingly, mesenchymal stem cell vesicles did not induce a better wound healing in our hands, although they are general considered to be anti-inflammatory. However, the anti-inflammatory action may not directly occur on the level of cell migration, but involve cytokine release and the interplay between different cell types.

2.4. Immunomodulatory effects of Lactobacillus MVs and BPs are dependent on the bacterial culture conditions

Wound healing is orchestrated by the release of inflammatory mediators. Next, we examined the effect of the MVs and the BP on primary human immune cells by measuring their effect on the cytokine production of peripheral blood mononuclear cells (PBMCs). Reduced cytokine release could be also linked to reduced cell survival. However, microscopic control of cell morphology, attachment and density revealed no influence of MV or BP treatment on these parameters excluding artifacts of reduced viability in the cytokine quantification (Supplementary Fig. S5). Furthermore, we previously showed that unmodified microparticles did not influence cytokine release [23]. Tumor necrosis factor (TNF) and interleukin-10 (IL-10) were chosen as readout parameters based on their pro-inflammatory and regulatory action, respectively, in wound healing, and LPS served as pro-inflammatory stimulus and comparator to assess relative changes.

The LPS-induced release of TNF was inhibited by treatment with MVs derived from anaerobic cultures of both *L. casei* and *L. plantarum*, with a slight reduction by the equivalent BPs (Fig. 4a). The release of IL-10 showed a tendency of reduction. In general, we observed a higher standard deviation than observed in other experiments. However, this was expected as the primary PBMCs show a high donor variability with respect to both stimulation by LPS, and the release of cytokines. We subsequently calculated the ratio of IL-10 and TNF because it has been reported to be an important predictor for wound healing. A higher IL-10 to TNF ratio was shown to correlate with healing outcomes in various conditions such as coronary artery disease, infections, and wound healing before. Tsurimi et al. demonstrated that an increase in this marker leads to a better healing outcome in burn wounds of adult patients [40–43]. Here, we detected elevated IL-10/TNF ratios for the anaerobic MVs from both strains, microparticles from the pH 6.5 culture, and the anaerobic *L. plantarum* conditions (Fig. 5e).The immune modulatory effects of *Lactobacillus* MVs have been demonstrated in the past [44,45]. To take the donor variability into account we calculated the IL-10/TNF ratio as measure of the anti-inflammatory action. We observed the strongest anti-inflammatory effect for the MVs from anaerobic cultures of both *Lactobacillus* strains. Interestingly, a similar trend was observed for *L. plantarum* pH 6.5 BPs and anaerobic BPs. Combining these observations with the findings made in the proteomics

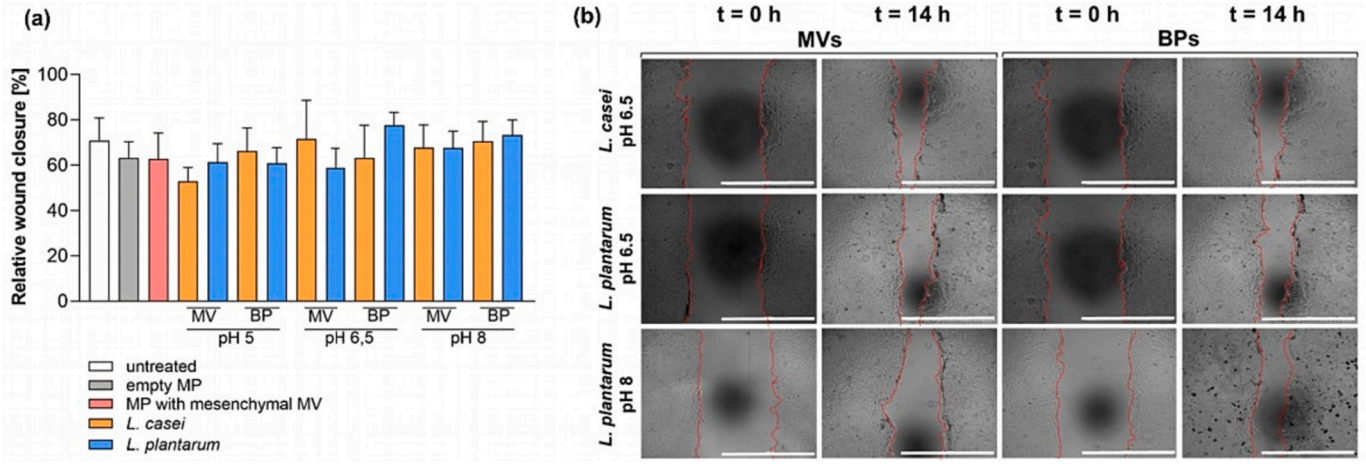

Fig. 4. Scratch assay results obtained from keratinocyte cell line HaCaT. (a) HaCaT cells were grown to confluence, incubated with mitomycin (2 μg/ml) for 2 h to exclude cell proliferation, and subjected to automated scratch for high reproducibility. Subsequently, cells were incubated with MVs, BPs, the empty microparticles (negative control), or extracellular vesicles from mesenchymal stem cells (positive control). Images were automatically taken every 2 h, and wound percentage of wound closure was determined after 14 h in comparison to an untreated control. (b) Representative images of the scratch after $t = 0$ h and $t = 14$ h for selected conditions are shown. The red lines indicate the borderline between cell edges and the cell-free area; scale bars indicate 1000 μm. Quantitative data are shown as means + SD calculated from six independent experiments. (For interpretation of the references to colour in this figure legend, the reader is referred to the web version of this article.)

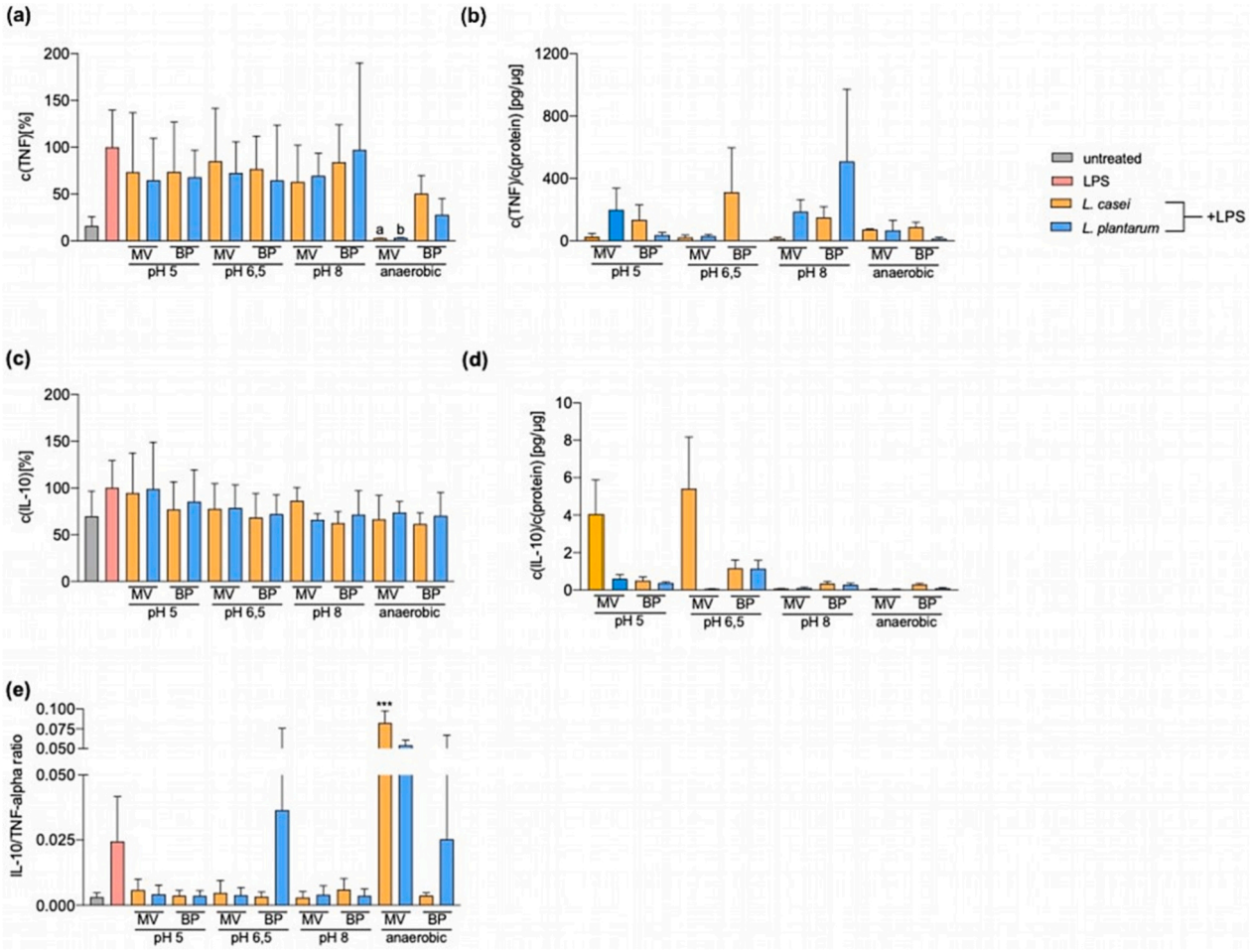

Fig. 5. Influence of the MVs on peripheral blood mononuclear cells. PBMCs were incubated with 1 µg/ml of lipopolysaccharide (LPS) and the MVs or BPs, respectively, for 4 h. The cytokine release of TNF and interleukin-10 to the supernatant were determined using ELISA. (a) TNF, data shown as a percentage, normalized to the inflamed control (average of LPS) to allow better comparability of effects induced my BPs. (b) IL-10, data shown as a percentage, normalized to the inflamed control (average LPS), and (c) IL-10/TNF ratio. Quantitative data are shown as means + SD calculated from three independent experiments. Statistical differences were analyzed by ANOVA followed by Dunnett's post-hoc test. ***$p < 0.001$, a: $p = 0.0516$, b: $p = 0.0534$.

characterization, we conclude that the changes observed in the proteins included in the MVs have a considerable impact on the biological effect of the MVs. We hypothesize that the 22 proteins found for *L. plantarum* both in the pH 6.5 and the anaerobic culture MVs are contributors to the biomimetics' anti-inflammatory effect. For *L. casei*, a similar pattern was observed, and the main contributors to the anti-inflammatory effect appear to be most expressed in pH 6.5 and in the anaerobic culture. Interestingly, for the anaerobic culture from both strains, we found that the BPs were less active in suppressing inflammation than the MVs. However, the BPs resembling a larger particle similar in size to bacteria. Thus, this physical stimulation *per se* could account for this weaker suppression, and requires further investigations.

In conclusion, culture of *L. plantarum* at pH 6.5 resulted in the highest concentration of MVs, which were already proven to improve healing in an intestinal cell line model after inflammation-induced barrier damage [23]. Further, these MVs showed the highest loading degree in BPs and the highest anti-inflammatory potential. Thus, MVs and BPs derived from *L. plantarum* pH 6.5 seemed to be the most promising candidates for initial *in vivo* experiments.

2.5. In vivo testing of MVs and BPs in hydrogel formulations

Essential prerequisites for the application of MVs and BPs on wounds are efficient delivery and deposition. Therefore, MVs and BPs were formulated into a hydrogel using a readily available pharmacopoeia hydroxyethyl cellulose (HEC) gel of 1% and 2.5% concentration. The same hydrogel mixed with phosphate-buffered saline was used as a negative control (hydrogel). Prior to animal experimentation, the release of fluorescently stained MVs from the gel was verified using fluorescence-assisted nanoparticle tracking analysis. A fast release of the MVs could be detected within 12 h and from both formulations (Supplementary Fig. S6), which confirmed that the hydrogel did not hamper the particle release and that no additional fixation in the wound bed would be required to allow efficient delivery.

We finally tested our formulations in a full-thickness mouse-tail *in vivo* wound model to get first indications regarding the applicability and safety of the MVs and BPs. Over the course of 30 days, changes of the wound and the tail were monitored, followed by detailed histological assessment. This model allows for sequential measurements and better clinical monitoring of the wound because only short hair but not fur is growing on the animal's tail [46]. Most importantly, the wound closure occurs without shrinkage from the wound edges and within a period comparable to human settings [47].

In our model, tail width and wound width served as surrogates to assess the inflammation, which occurs during the wound healing process, modulated by edema and exudate formation. The tail width increased by 1 mm during the first week for the empty hydrogel treated animals while the increase was lower with an earlier recovery in MV and BP hydrogel treated animals, respectively (Supplementary Fig. S7a). The wound width increased by >1 mm after 1 week for the empty hydrogel

treated animals as well as the group treated with MV loaded hydrogel. The BP hydrogel led to a quick reduction in the wound width, which was significantly different already at day 5 post wounding compared to the other groups (Fig. 6a,b). While for the BP loaded hydrogel the initial width was restored already 12 days after wounding, it took between day 23 and 24 for empty hydrogel and the MV-loaded hydrogel. The length and width of the inner wound area served as macroscopic measurements of re-epithelialization. Hydrogel treated wounds showed the fastest reduction in wound length (Supplementary Fig. S7b). However, the allover wound closure time is not affected (Supplementary Fig. S7c). Especially, MV hydrogel treated animals showed a significantly reduced reduction in wound length within the first two weeks after wounding (Supplementary Fig. S7b). Interestingly, the inner wound width was faster reduced in BP hydrogel treated animals compared to hydrogel or MV treated animals (Fig. 6c, significance between MV and BP hydrogel treatment). Thus, BP loaded hydrogels seem to dampen the inflammatory response during the wound healing process, supporting faster re-epithelialization.

To gain further evidence, we performed detailed (immune)histological analyses. Restoration of the damaged tissue is one criterion for advances in wound care. None of the treatments reduced the increase of the epidermis thickness (Fig. 6d, Supplementary Fig. S7d). The structured epidermis is characterized by a basal cell layer (*Stratum basale*), which are the source for the keratinocytes forming the *Stratum spinosum* and Stratum *granulosum*. BP-loaded hydrogel reduced the percentage of non-structured epidermis within the wound site significantly in comparison to hydrogel treated wounds, while MV-loaded hydrogel showed a high variability (Fig. 6e) [48]. An increased dermal thickness correlates to a higher infiltration with fibrocytes and was shown to indicate a higher risk of scarring [49]. For the mice treated with BP loaded hydrogel, a significant decrease of dermis thickness compared to treatment with hydrogel and the MV loaded hydrogel, respectively, was observed (Fig. 6f). Additional measures of scare formation are the cell number (indication of hypertrophy) and the collagen deposition. Therefore, cells within the wounded sites (hematoxylin-eosin staining) and the collagen deposition (Ladewig trichrome staining) were automatically counted. All three treatments showed an increase of cellularity, but without significant differences amongst the treatment groups (Fig. 6g). Further, we determined the total wound area and calculated the overall cell number, again without obvious differences

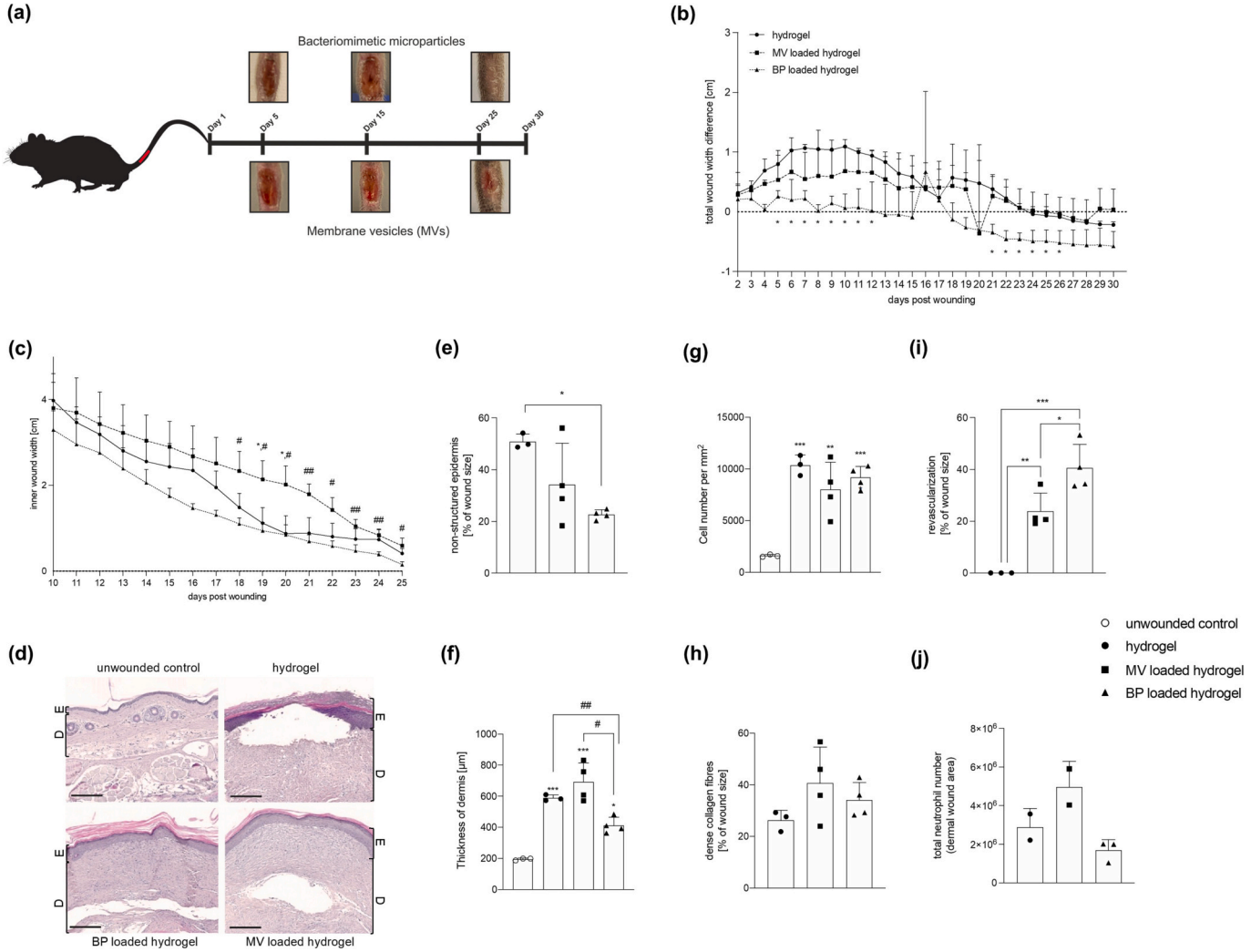

Fig. 6. Full-thickness wound healing mouse model. Full-thickness wounds of 10 × 3 mm size were set in the tails and covered with either hydrogel, MV loaded hydrogel or BP loaded hydrogel (MVs obtained from L. *plantarum* cultured at pH 6.5). Wound size and tail width were measured each day. (a) Representative pictures of the wounds at different time points after wounding. (b) Differences in total wound width. (c) *Re*-epithelialized wound area. (d-j) Hematoxylin-eosin (exemplary images shown in d, scale bare indicate 200 µm), Ladewig trichrome and immunohistochemical stainings were analyzed for epidermal structure (e), thickness of dermis (f), cell density (g), collagen structure (h), neovascularization (i) and neutrophil number (j). Quantitative data are shown as means + SD calculated ($n = 3$–4 in a-j, $n = 2$–3 in j). Statistical differences were analyzed by One-way ANOVA followed by Tukey's post test. Asterisks indicate differences to the unwounded control, hashes between treatment groups. $^{*,\#}p < 0.05$, $^{**,\#\#}p < 0.01$, $^{***}p < 0.001$.

(Supplementary Fig. S7e). Similarly, no differences in collagen deposition to the dermal wound area were observed (Supplementary Fig. 7f,g). Nevertheless, dermal thickness has been described as a risk factor for hypertrophic scarring [50]. The healthy tail dermis is characterized by dense and organized collagen fibers. MV and BP hydrogel, respectively, treated wounds showed a tendency towards an increase of recovered collagen organization at the wound edges in comparison to hydrogel treated wounds, which was not reaching significance (Fig. 6h). However, with respect to the 3R only low animal numbers were used in this initial testing, potentially not allowing for the observation of slight differences. Furthermore, formation of the granulation tissue and re-epithelialization are part of the proliferation phase in wound healing. The maturation phase, including the decision between resolution of the granulation tissue and the scar formation, occurs in a time frame of several month to one year. This phase is not covered by the used basic model and would require further investigation in, for example, chronic or diabetic wound healing models. One additional parameter of wound healing is the induction of re-vascularization. Within hydrogel treated wounds, no revascularization sites were detected in the histological staining. However, both MV and BP loaded hydrogels induced revascularization, with BPs showing a higher efficiency (Fig. 6h).

Our *in vitro* experiments showed a change of the IL10 to TNF ratio upon treatment with MVs and the bacteriomimetic microparticles, which could change the presence of inflammatory cells within the wound area. Based on the late time point, TNF release into the wound are could not be detected (data not shown). Further, we did not observe changes in $CD68^+$ macrophage numbers or $CD3^+$ T lymphocyte infiltration after full wound closure (Supplementary Fig. S7h-j). In general, macrophage density always decreases after wound closure [51]. Thus, it might be that the change in the inflammatory behavior accounts in more early phases of the wound healing process, which may also explain the lack of neutrophil detection (early phase markers). Indeed, treatment with BP loaded hydrogel resulted in an early resolution or less pronounced inflammatory response as indicated by wound width and less exudate during experiments. Neutrophils are beneficial for wound healing preventing wounds from infection, but the damage by the proteolytic activity of protesases can lead to delayed healing and scar formation [55]. Wound treated with MV loaded hydrogel showed a slight increase in myeloperoxidase (MPO) as neutrophil marker in comparison to hydrogel treated wounds, whereas the number of neutrophils was reduced by BP hydrogel treatment (Fig. 6j, $p = 0.0361$). These findings are in line with the delayed re-epithelialization in MV hydrogel *versus* BP hydrogel treated wounds (Fig. 6c).

Taking all evidences from this initial *in vivo*-testing together, the application of bacteriomimetic hydrogel seems to be save and offers a therapeutic potential to care delayed wound healing. This initial study stimulates for future investigations in more complex wound healing models like diabetic ulcera or infected wounds.

3. Conclusion

In this study, we explored a bacteriomimetic hydrogel as therapeutic system in the context of wound healing. We harvested membrane vesicles from two *Lactobacillus* strains – *L. casei* and *L. plantarum* – and showed their cell tolerability and their anti-inflammatory effects. We subsequently designed a novel non-proliferating bacteriomimetic therapeutic system and revealed its promising anti-inflammatory effects *in vitro*, and its capability to improve wound healing and decrease scar formation in an *in vivo* full thickness mouse model.

In recent years, various reports have emerged, highlighting the therapeutic effects of probiotic bacteria in wound healing, *e.g.*, hydrogels with live-bacteria [24]. *Lactobacillus reuteri* bacteria were further used as drug delivery vectors in a similar model [52]. Comparable approaches were explored in recent years, using heat-killed or lysed bacteria [19,53]. Within our present study, we showed that wound healing can also be increased using the bacteriomimetic microparticles, reducing the risk of live bacteria treatment or reaction to other bacterial components and offering novel treatment options for non-healing wounds and immunocompromised patients. Nevertheless, the effect could be improved by packing the vesicles more densely on the microparticle surface. In addition, dose-response studies may reveal enhanced anti-inflammatory activity. Further studies should also include bacteriomimetic hydrogel testing in the context of other cutaneous diseases involving inflammation such as autoimmune diseases of the skin, as well as further developing the system using biodegradable polymers as carrier materials.

4. Experimental section

4.1. Cell culture

HaCaT cells were cultured in Dulbecco's modified eagle medium (Gibco, USA) supplemented with 10% fetal calf serum (FCS) (Gibco, USA). Medium was exchanged every 2–3 days. Cells were passaged to a new flask every 7 days, when 80–90% confluence was reached.

THP-1 cells were cultured in a suspension culture in RPMI (Gibco, USA) medium supplemented with 10% FCS (Gibco, USA). Every 3–4 days, 10^6 cells were passaged to a new T75 flask and supplemented with 10 ml of fresh medium.

4.2. Bacterial culture

Lactobacillus casei DSM20011 (DSMZ, Germany) were cultured in deMan-Rogosa-Sharpe (MRS) medium (Carl Roth). Initially, bacteria were cultured on an MRS agar plate for 4 days at a temperature of 37 °C under a 5% CO_2 atmosphere. This plate was then stored at 4 °C for up to 4 weeks. For liquid cultures, 2 single colonies were used to inoculate 100 ml of liquid MRS medium. Liquid cultures were then placed in an incubator without shaking at a temperature of 37 °C and allowed to grow for 48 h.

Lactobacillus plantarum NCIBM 8826 (NCIBM, UK) were cultured in deMan-Rogosa-Sharpe (MRS) medium (Carl Roth, Germany). Initially, bacteria were cultured on an MRS agar plate for 2 days at a temperature of 30 °C. This plate was then stored at 4 °C for up to 4 weeks. For liquid cultures, 2 single colonies were used to inoculate 100 ml of liquid MRS medium. Liquid cultures were then placed in an incubator shaking at a temperature of 30 °C and allowed to grow for 48 h.

For the different pH-conditions medium pH was adjusted to pH 5 or pH 8 using HCl and NaOH. Regular medium had a pH value of 6.5. For anaerobic culture, the medium was additionally supplemented with 0.05% sodium thioglycolate, and the incubations were performed in airtight bottles completely filled with medium.

4.3. EV isolation

After 48 h of growth, bacteria were separated from the supernatant using centrifugation at 9500 x*g* for 5 min. The bacterial pellet was discarded, and supernatants were further purified using 0.45 μm pore size vacuum filtration using Stericup-HV 150 ml Durapore PVDF 0.45 filter bottles, (Merck, Germany). Then, the filtered supernatants were centrifuged for 2 h at 4 °C at a centrifugal force of 100,000 x*g* using an ultracentrifuge with a Type45 Ti fixed angle rotor. (Beckmann, USA). After ultracentrifugation, supernatants were discarded and the pellets, containing EVs and co-pelleted proteins were resuspended in 400 μl of filtered phosphate-buffered saline.

Resuspended pellets were further purified from co-pelleted proteins using size-exclusion chromatography. Pellets were transferred to a chromatography column containing 40 ml of Sepharose CL-2B (Gibco, USA) and eluted with filtered phosphate-buffered saline. Fractions of each 1 ml were collected.

4.4. Cryoelectron microscopy

3 μL of MV sample was transferred to a copper grid and blotted for 2

s. The grid was then plunged into undercooled liquid ethane (−165 °C; Gatan Cryoplunge3) and transferred under liquid nitrogen to a cryo-TEM sample holder (Gatan model 914). Low-dose bright-field images were acquired at −170 °C on a JEOL JEM-2100 LaB6 Transmission Electron Microscope equipped with a Gatan Orius SC1000 CCD camera.

4.5. Proteomics

4.5.1. Lysis of the MVs

To determine the proteins contained inside the MVs, MVs were diluted to 1×10^{11} particles/ml for L. *plantarum* and 1×10^{12} particles/ml for *L. casei*, and lysed using a buffer containing 1% Triton-X 100 (SigmaAldrich, USA) with 50 mM Tris-HCl (Serva, Germany) and 150 mM NaCl for 4 h cooled to 0 °C with intermediate vortexing every hour.

4.5.2. Filter assisted protein digestion

Lysed samples were transferred onto a filter tube with a MWCO of 10 kDa. Excess liquid was removed centrifuging at 8000 x g at 4 °C. Proteins were then reduced using 450 µl of a 1 M solution of Dithiothreitol in 0.1 M ammonium hydrogen carbonate for 45 min at 56 °C. After the liquid was removed *via* centrifugation, 450 µl of alkylation buffer (0.5 M iodoacetamide in water) was added and the mixture was incubated for 30 min at RT. The liquid was removed again, and, after two washing steps with 50 mM ammonium hydrogen carbonate. Next, 450 µl of digestion buffer (49 ng/ml of Trypsin in 50 mM of ammonium hydrogen carbonate) were added and the mixture was incubated overnight at 37 °C. On the next day, the digested peptides were centrifuged into an Eppendorf tube, and the filter was washed twice with 300 µl of 5% formic acid. Next, the liquid was removed using a vacuum centrifuge at 60 °C for 2 h. The dried peptides were dissolved in 10% formic acid and stored at −20 °C for LC-MS analysis.

4.5.3. LC-MS/MS analysis

The tryptic digests are analyzed on a Dionex UltiMate 3000 rapid separation liquid chromatography (RSLC) system (Thermo Fisher Scientific, Waltham, MA, USA) coupled to a Bruker timsTOF, a high-resolution hybrid trapped ion-mobility spectrometry-quadrupole time-of-flight mass spectrometer equipped with a high-resolution electrospray ionization (HRESI) source (Bruker Daltonics, Billerica, MA, USA). Separation of 10 µl sample was achieved with a gradient of acetonitrile with 0.1% formic acid (B) in ddH2O with 0.1% formic acid (A) on an ACQUITY BEH C18 column (100 mm × 2.1 mm, 1.7 µm dp) (Waters, Eschborn, Germany) equipped with a Waters VanGuard BEH C18 1.7 µm guard column at a flow rate of 0.6 ml/min and 45 °C. The initial gradient was held at 5% B for 1 min and then elevated to 45% B within 20 min. After that, the B level was elevated to 95% within 3 min and held there for 5 min. Finally, the gradient was ramped back to 5% B in 1 min and re-equilibrated for the next injection for 1 min. Detection is performed by a diode array detector at 200–600 nm. The LC flow is split into 75 µl/min before entering the mass spectrometer, which was externally calibrated to a mass accuracy <1 ppm and a collisional cross section (CCS) accuracy <0.5%. Mass spectrograms were acquired in parallel accumulation and serial fragmentation (PASEF) mode ranging from 100 to 1700 *m/z* and 0.6–1.6 V*s/cm2 1/k0 in positive MS mode. Source parameters are set to 500 V end-plate offset, 4000 V capillary voltage, 1.5 bar nebulizer gas pressure, 6 L/min dry gas flow and 200 °C dry gas temperature. Ion transfer and quadrupole parameters were set to 350 VPP funnel 2 RF, 400 VPP multipole RF, 5 eV ion energy and 100 m/z low-mass cut-off. TIMS settings are 350 VPP funnel 1 RF and 250 V collision cell in. Collision cell was set to 80 µs transfer time, 1200 VPP collision RF and pre-pulse storage was set to 12 µs. PASEF parameters were set to 10 MS/MS scans (total cycle time: 1.89 s), charge range 0–5, active exclusion for 0.4 min, scheduling target intensity was set to 10,000, intensity threshold was set to 1000 and CID collision energy is 20–59 eV, depending on precursor mass and charge. The HPLC-MS system was operated by HyStar 6.0.30.0 (Bruker Daltonics, Billerica, MA, USA), and LC chromatograms, as well as UV spectra and mass spectrograms were analyzed with DataAnalysis 5.3 (Bruker Daltonics, Billerica, MA, USA).

4.5.4. Data analysis

The acquired raw data were submitted to PEAKS X Pro, PEAKS Studio 10.6 (Bioinformatics Solutions, Waterloo, ON, Canada) to search against FASTA protein databases constructed for *Lactobacillus casei* DSM 20011 (UniProt Proteome ID UP000015560) and *Lactobacillus plantarum* NCIMB 8826 (UP000000432). For de-novo search, the mass error tolerance was set to 10 ppm and the fragment mass error tolerance to 0.1 Da. Trypsin was defined as digestion enzyme with three missed cleavages allowed. Variable modifications are carboamidomethylation of cysteine and oxidation of methionine, histidine and tryptophane allowing for 10 variable modifications per peptide. PTM search was conducted with the default 312 built-in modifications allowing for 3 variable modifications per peptide. Maximum false discovery rates (FDRs) were set to 5%. Protein identifications were considered true when at least one unique peptide was identified per protein with a confidence score of –10IgP $\geq$ 20.

For protein identification, cultivation of Lactobacilli, EV isolation and sample preparation was performed in biological triplicates. Each replicate was analyzed by LC–MS/MS in technical duplicates, resulting in a total of six measurements per condition.

4.6. Coupling of MVs to microparticles

300 µl of MVs as harvested were mixed with 700 µl of phosphate-buffered saline and 10 µl of pre-washed Aldehyde/sulfate latex beads (ThermoFisher, USA). The mixture was incubated for 16 h while shaking at 300 rpm. Afterward, the coated microparticles were pelleted by centrifugation of 5 min at 5000 xg and washed using 1 ml of phosphate-buffered saline. This procedure was then repeated twice. Then, the coated particles were suspended in 1 ml of phosphate-buffered saline. For electron microscopy, the coated microparticles were additionally washed three times with deionized water.

4.7. Determination of protein content

To determine the protein content, the QuantiPro BCA assay kit (Merck, Germany) was used according to the manufacturer's recommendations. In brief, 150 µL of each SEC fraction was pipetted into a 96-well plate and mixed well with 150 l of QuantiPro BCA assay working reagent (Sigma Aldrich, USA). Bovine serum albumin standard was used for calibration. After incubation for 1 h at 60 °C, the absorbance at 562 nm was measured using a plate reader (Tecan, USA). The amount of MVs on the microparticles was determined using the following equation:

$$c(protein\ on\ MPs) = c(protein\ in\ SEC\ fraction) - c(protein\ in\ supernatant) \quad (1)$$

$$MVs\ on\ microparticles\% = \{\{[[c(\text{particle/mL of MV in formulation}) * c(\text{protein on MP surface})] / c(\text{protein in MV})] / c(\text{particle/mL of MPs in formulation})\} / (\text{surface of single MP } m^2 / \text{circular area of a 100 } nm\ MV\ in\ m^2)\} \ x\ 100$$

With c(MPs in formulation) = $1.43*10^7$/ml (determined using the formulae on the ThermoFisher website); c(MV average) was averaged to $3.33*10^{10}$/ml based on nanoparticle tracking analysis [23] The instrument used was a NanoSight (Malvern Panalytical, Malvern, UK) under constant settings (camera level: 15, detection threshold: 5) for every measurement. The NTA 3.3 software was used for analysis; surface of single MP m^2/ circular area of a 100 nm MV in m^2 was calculated with aldehyde/sulfate latex beads of 4 μm and 100 nm MVs: calculated factor = 22.89 m^2/ 0.00785 m^2 = 2916.

4.8. Scanning electron microscopy

A 3 μl volume of each sample was transferred to a silica wafer and allowed to dry at RT for 2–3 h. Samples were then sputtered with a 10 nm layer (Quorum Q150R ES) of gold and imaged under high vacuum using an accelerating voltage of 5–10 kV and a beam current of 1.978 pA (Zeiss EVO MA15 LaB6).

4.9. Viability assay

Cells were seeded into 96-well plates, two types of cells were used, namely HaCaT (keratinocyte-like) and dTHP-1 (differentiated THP-1, macrophage-like). For the assays using HaCaT cells, approximately 2 × 10^4 HaCaT cells suspended in 200 μl of DMEM, supplemented with 10% FCS and 1% nonessential amino acid (Invitrogen, Waltham, MA). For the assays using dTHP-1 cells, THP-1 cells were seeded at a density of 100,000 cells per well in RPMI medium supplemented with 10% FCS and 7.5 ng/ml phorbol 12-myristate 13-acetate (PMA).

After allowing the cells to grow for 48 h, the medium was aspirated, and 100 μl of fresh medium (without FCS, in order to prevent interference of FCS with the LDH assay) was added, followed by the addition of 100 l of the sample. The controls used were death-control (medium supplemented with 2% TritonX-100) and live-control (PBS).

Cells were incubated with EVs of the highest-concentrated SEC fraction (≈5 × 10^{11} for *L. plantarum* and ≈5 × 10^{12} for *L. casei* EVs ml^{-1}) and three serial 1:10 dilutions for 24 h. PrestoBlue (ThermoFisher Scientific, Waltham, MA) reagent was diluted 1 in 10 in the respective medium of the cells. After incubation for 24 h, 100 μl of the medium was sampled for analysis by the LDH-assay. The remaining medium was aspirated and cells were supplemented with 100 μL of the diluted PrestoBlue reagent. After 20 min of incubation at 37 °C, the fluorescence of the emerging fluorescent dye was measured.

A 100 μl volume of the supernatant was mixed with 100 μl of LDH-reagent (Roche), prepared according to the supplier's protocol. After an incubation time of 5 min at RT, the absorbance of the solution was measured at λ = 492 nm.

4.10. Scratch assay

For live-cell analysis of scratch-induced wound closure, 2 × 10^4 cells per well were seeded on collagen G (40 μg/ml) (Biochrom, Germany) coated 96-well plates near confluence and allowed to grow overnight in standard medium. At confluence, cells were pre-treated for 2 h with mitomycin (5 μg/ml) to inhibit cell proliferation followed by 3 times washing with PBS. Subsequently, a defined scratch was performed in each well using the certified BioTec autoscratch (BioTec, Highland Park, USA) for 96-well plates ensuring an equal scratch of around 1.2 cm2 in each well, as described previously [54]. The medium was removed and 100 μl standard medium were added to the wells. The closure of the wounded area was monitored using the Lionheart (FX) Automated Microscope system (BioTec, Highland Park, USA) by taking images of each well every 2 h over a period of 24 h. The reduction of wound width was determined over time using the Gen5 software version 3.05.11. For accurate measurement of control cells, wound closure was determined after 14 h. An automated primary mask that quantifies the area in the image containing cells was used to quantify the progression of cell migration.

4.11. Isolation of peripheral blood mononuclear cells (PBMCs) from Buffy Coats

We isolated PBMCs from adult healthy blood donors (Blood Donation Center, Saarbrücken, Germany). Human material use and handling was approved by the local Ethics Committees (permission no. 173/18; State Medical Board of Registration, Saarland, Germany). PBMCs were isolated using density gradient centrifugation with Lymphocyte Separation Medium 1077 (Promocell, C-44010) and Leucosep tubes (Greiner Bio-One, 227,290) according to the supplier's protocols.

For cytokine analysis, cells were incubated with the respective treatments for 6 h at 37 °C; afterwards supernatants were collected and stored until analysis at −80 °C. The concentration of the cytokines was determined using Human IL-10 ELISA Set (Diaclone, Besançon, France) and Human TNF-α ELISA Set (Diaclone, Besançon, France), the experimental procedure was carried out according to the supplier's protocols. Raw data was normalized to the cytokine concentration of the inflamed lipopolysaccharide controls.

4.12. Preparation of the EV-containing hydrogels

Hydrogels were prepared using a simple method derived from the German pharmacopoeia (DAB). Briefly, hydroxyethyl cellulose (1% or 2.5% respectively) was mixed with glycerol (20%) until an even mixture was achieved. Then, ultrapure water (MilliQ) was added, and the mixture was allowed to swell for 16 h at 4 °C. The gel was then sterilized in an autoclave for 20 min at 121 °C at a pressure of 200 kPa. Afterward, any evaporated water was re-added. The gels were then mixed with the MVs or microparticles (1 × 10^{11} particles/ml for *L. plantarum* and 1 × 10^{12} particles/ml for *L. casei*) and mixed in a 1:1-ratio with the pre-prepared hydrogel. Phosphate-buffered saline mixed with hydrogel was used as control.

4.13. In vivo experiments

Animal experiments were performed with 8-weeks old male mice on C57BL76 background and approved by the local authorities (20/2021 LAV Saarland). Mice were anesthetized for 30 min with 100 mg/kg BW ketamine and 5 mg/lg BW xylazine and a skin flap of 10 × 3 mm approximately 0.5 cm distal to the tail base. Thereby and by holding in single cages, removal of the hydrogel was avoided. A template built from scalpels ensured consistency in length, width and depth of the wounds. Wounds were covered with 50 μl hydrogel containing extracellular vesicles obtained from *Lactobacillus plantarum* (MV loaded hydrogel) or microparticles coated with these vesicles (BP loaded hydrogel). Hydrogel without supplementation served as control treatment. The hydrogel entered the open wound during the wake-up phase avoiding displacement or removal by movement. Licking was avoided by the location of the wound and single holding of the animals. During the first three days, borgal (2 mg/ml) was given in drinking water as prophylactic antibiotic medication. Mice received 0.1 mg/kg buprenorphine *i.p.* twice a day and 1 mg/kg in drinking water overnight for analgesia. Wounds and tail sides were photographed daily and measured for wound length, wound width, and tail width using a sliding caliper. Mice were sacrificed after complete wound closure (28 to 30 days) and probed for tail tissue. The wound was fixed for 48 h in RotiFix® (Roth, Germany) and embedded in paraffin. Tissue was decalcified, 5 μm sections were subjected to hematoxylin–eosin (HE) and Ladewig trichrome staining following established protocols, and images were taken using the Axioscan Z1 slide scanner (Zeiss, Germany). Measurements and cell counts in the wound area were performed and analyzed using Zen blue and AxioVision 6.4.1 software (Zeiss).

4.14. Immunohistological staining of mouse tissue sections

Sections were deparaffinized, rehydrated, and subjected to antigen retrieval in TRIS/EDTA buffer (pH 9). After blocking in PBS supplemented with 1.5% normal serum, slices were incubated with rabbit anti-mouse CD68 (macrophages), CD3 (lymphocytes) or MPO (neutrophils), washed in PBS, followed by biotin-goat-anti-rabbit and streptavidin-HRP. Antibody binding was visualized by AEC (3-Amino-9-Ethylcarbazole) HRP reaction, and nuclei were counterstained with hemalaun. At least, five quadrants per wound field were counted in a blind manner.

4.15. Statistical analyses

Statistics were calculated and graphs were created using the software GraphPad Prism. Plotted values represent the mean value of all performed replicates, error bars indicate the standard deviation. Used statistical tests are indicated in the figure legend. A p-value below 0.05 was regarded as significant.

CRediT authorship contribution statement

Thomas Kuhn: Writing – original draft, Funding acquisition, Formal analysis, Data curation. **Ahmad Aljohmani:** Formal analysis, Data curation. **Nicolas Frank:** Formal analysis, Data curation. **Lina Zielke:** Data curation. **Mina Mehanny:** Data curation. **Matthias W. Laschke:** Formal analysis, Resources. **Marcus Koch:** Data curation. **Jessica Hoppstädter:** Writing – review & editing, Methodology. **Alexandra K. Kiemer:** Resources, Project administration, Methodology. **Daniela Yildiz:** Writing – review & editing, Supervision, Project administration, Methodology, Formal analysis, Data curation, Resources. **Gregor Fuhrmann:** Writing – review & editing, Writing – original draft, Visualization, Validation, Supervision, Resources, Project administration, Funding acquisition, Conceptualization.

Declaration of Competing Interest

None.

Data availability

Data will be made available on request.

Acknowledgements

We thank U. Boehm and P. Wartenberg for use of and technical assistance with the slide scanner (DFG-Nr. Inst. 256/434-1 to UB). We thank J. Becker and M. Rieseweber for technical assistance. We thank the AG Krasteva-Christ for the use of microtome, and Dr. Jennifer Munkert for her help with calculating the surface coverage of microparticles. The authors acknowledge financial support by Studienstiftung des Deutschen Volkes and VW-Stiftung.

Appendix A. Supplementary data

Supplementary data to this article can be found online at https://doi.org/10.1016/j.jconrel.2023.12.011.

References

[1] Y. An, W. Wei, H. Jing, L. Ming, S. Liu, Y. Jin, Bone marrow mesenchymal stem cell aggregate: an optimal cell therapy for full-layer cutaneous wound vascularization and regeneration, Sci. Rep. 5 (1) (2015) 1–12, https://doi.org/10.1038/srep17036.
[2] J. di Domizio, C. Belkhodja, P. Chenuet, A. Fries, T. Murray, P.M. Mondéjar, O. Demaria, C. Conrad, B. Homey, S. Werner, D.E. Speiser, B. Ryffel, M. Gilliet, The commensal skin microbiota triggers type I IFN–dependent innate repair responses in injured skin, Nat. Immunol. 21 (9) (2020) 1034–1045, https://doi.org/10.1038/s41590-020-0721-6.
[3] H. Yin, X. Li, S. Hu, T. Liu, B. Yuan, H. Gu, Q. Ni, X. Zhang, F. Zheng, IL-33 accelerates cutaneous wound healing involved in upregulation of alternatively activated macrophages, Mol. Immunol. 56 (4) (2013) 347–353, https://doi.org/10.1016/j.molimm.2013.05.225.
[4] S. Dekoninck, C. Blanpain, Stem cell dynamics, migration and plasticity during wound healing, Nat. Cell Biol. (2019) 18–24, https://doi.org/10.1038/s41556-018-0237-6. Nature Publishing Group January 2.
[5] T.J. Koh, L.A. DiPietro, Inflammation and wound healing: the role of the macrophage, Expert Rev. Mol. Med. 13 (2011), e23, https://doi.org/10.1017/S1462399411001943.
[6] G.C. Gurtner, S. Werner, Y. Barrandon, M.T. Longaker, Wound repair and regeneration, Nature 453 (7193) (2008) 314–321, https://doi.org/10.1038/nature07039.
[7] C.K. Sen, G.M. Gordillo, S. Roy, R. Kirsner, L. Lambert, T.K. Hunt, F. Gottrup, G. C. Gurtner, M.T. Longaker, Human skin wounds: a major and snowballing threat to public health and the economy, Wound Repair Regen. 17 (6) (2009) 763, https://doi.org/10.1111/J.1524-475X.2009.00543.X.
[8] C.K. Sen, Human wounds and its burden: an updated compendium of estimates, Adv. Wound Care (New Rochelle) 8 (2) (2019) 39–48, https://doi.org/10.1089/WOUND.2019.0946.
[9] B. Nink-Grebe, D. Rüttermann, Maier-Hasselmann, S3-Leitlinie Zur Lokaltherapie Chronischer Wunden Bei Patienten Mit Den Risiken Periphere Arterielle Verschlusskrankheit, Chronische Venöse Insuffizienz Und Diabetes Mellitus, Z. Wundheil. 1 (2012) 4–6.
[10] A. Leung, T.M. Crombleholme, S.G. Keswani, Fetal wound healing: implications for minimal scar formation, Curr. Opin. Pediatr. 24 (3) (2012) 371, https://doi.org/10.1097/MOP.0B013E3283535790.
[11] N. Lunjani, S. Ahearn-Ford, F.S. Dube, C. Hlela, L. O'Mahony, Mechanisms of microbe-immune system dialogue within the skin, Genes Immun. 22 (5) (2021) 276–288, https://doi.org/10.1038/s41435-021-00133-9.
[12] G. Wang, E. Sweren, H. Liu, E. Wier, M.P. Alphonse, R. Chen, N. Islam, A. Li, Y. Xue, J. Chen, S. Park, Y. Chen, S. Lee, Y. Wang, S. Wang, N.K. Archer, W. Andrews, M.A. Kane, E. Dare, S.K. Reddy, Z. Hu, E.A. Grice, L.S. Miller, L. A. Garza, Bacteria induce skin regeneration via IL-1β signaling, Cell Host Microbe 29 (5) (2021) 777–791.e6, https://doi.org/10.1016/J.CHOM.2021.03.003.
[13] P.W. O'Toole, J.R. Marchesi, C. Hill, Next-generation probiotics: the spectrum from probiotics to live biotherapeutics, Nat. Microbiol. (2017) 1–6, https://doi.org/10.1038/nmicrobiol.2017.57. Nature Publishing Group April 25.
[14] T. Didari, S. Solki, S. Mozaffari, S. Nikfar, M. Abdollahi, A systematic review of the safety of probiotics, in: Expert Opinion on Drug Safety, Taylor & Francis February, 2014, pp. 227–239, https://doi.org/10.1517/14740338.2014.872627.
[15] M. Toyofuku, N. Nomura, L. Eberl, Types and origins of bacterial membrane vesicles, Nat. Rev. Microbiol. (2019) 13–24, https://doi.org/10.1038/s41579-018-0112-2. Nature Publishing Group January 1.
[16] G. Fuhrmann, Diffusion and transport of extracellular vesicles, Nat. Nanotechnol. 15 (3) (2020) 168–169, https://doi.org/10.1038/s41565-020-0651-3.
[17] M. Kaparakis-Liaskos, R.L. Ferrero, Immune modulation by bacterial outer membrane vesicles, Nat. Rev. Immunol. 15 (6) (2015) 375–387, https://doi.org/10.1038/nri3837.
[18] L.P. Jahromi, G. Fuhrmann, Bacterial extracellular vesicles: understanding biology promotes applications as nanopharmaceuticals, Adv. Drug Deliv. Rev. 173 (2021) 125–140.
[19] W.H. Tsai, C.H. Chou, T.Y. Huang, H.L. Wang, P.J. Chien, W.W. Chang, H.T. Lee, Heat-killed lactobacilli preparations promote healing in the experimental cutaneous wounds, Cells 10 (11) (2021) 3264, https://doi.org/10.3390/cells10113264.
[20] D.H. Kim, S.Y.S.W.S. Kim, J.B. Ahn, J.H. Kim, H.W. Ma, D.H. Seo, X. Che, K. C. Park, J.J. Yong, H.C. Lee, J.Y. Lee, T. Il Kim, W.H. Kim, S.W. Kim, J.H. Cheon, *Lactobacillus plantarum* CBT LP3 ameliorates colitis via modulating T cells in mice, Int. J. Med. Microbiol. 310 (2) (2020), 151391, https://doi.org/10.1016/j.ijmm.2020.151391.
[21] E. Jacouton, F. Chain, H. Sokol, P. Langella, L.G. Bermúdez-Humarán, Probiotic strain Lactobacillus Casei BL23 prevents colitis-associated colorectal cancer, Front. Immunol. 8 (2017) 1553, https://doi.org/10.3389/fimmu.2017.01553.
[22] W. Kim, E.J. Lee, I.H. Bae, K. Myoung, S.T. Kim, P.J. Park, K.H. Lee, A.V.Q. Pham, J. Ko, S.H. Oh, E.G. Cho, *Lactobacillus plantarum*-derived extracellular vesicles induce anti-inflammatory M2 macrophage polarization in vitro, J. Extracell. Vesicles 9 (1) (2020), https://doi.org/10.1080/20013078.2020.1793514.
[23] T. Kuhn, M. Koch, G. Fuhrmann, Probiomimetics—novel *Lactobacillus*-mimicking microparticles show anti-inflammatory and barrier-protecting effects in gastrointestinal models, Small 16 (40) (2020) 2003158, https://doi.org/10.1002/smll.202003158.
[24] Z. Ming, L. Han, M. Bao, H. Zhu, S. Qiang, S. Xue, W. Liu, Living bacterial hydrogels for accelerated infected wound healing, Adv. Sci. 8 (24) (2021) 2102545, https://doi.org/10.1002/ADVS.202102545.
[25] L. Müller, T. Kuhn, M. Koch, G. Fuhrmann, Stimulation of probiotic Bacteria induces release of membrane vesicles with augmented anti-inflammatory activity, ACS Appl. Bio Mater. (2021), https://doi.org/10.1021/acsabm.0c01136. American Chemical Society May 17.
[26] M.L. Marco, M.C. De Vries, M. Wels, D. Molenaar, P. Mangell, S. Ahrne, W.M. De Vos, E.E. Vaughan, M. Kleerebezem, Convergence in probiotic *Lactobacillus* gut-adaptive responses in humans and mice, ISME J. 4 (11) (2010) 1481–1484, https://doi.org/10.1038/ismej.2010.61.

[27] C. Bäuerl, G. Pérez-Martínez, F. Yan, D.B. Polk, V. Monedero, Functional analysis of the P40 and P75 proteins from *Lactobacillus casei* BL23, J. Mol. Microbiol. Biotechnol. 19 (4) (2011) 231, https://doi.org/10.1159/000322233.
[28] A.P. Domínguez Rubio, J.H. Martínez, D.C. Martínez Casillas, F. Coluccio Leskow, M. Piuri, O.E. Pérez, *Lactobacillus Casei* BL23 produces microvesicles carrying proteins that have been associated with its probiotic effect, Front. Microbiol. 8 (SEP) (2017) 1783, https://doi.org/10.3389/fmicb.2017.01783.
[29] L. Müller, T. Kuhn, M. Koch, G. Fuhrmann, Stimulation of probiotic bacteria induces release of membrane vesicles with augmented anti-inflammatory activity, ACS Appl. Bio Mater. (2021), https://doi.org/10.1128/Spectrum.01273-21 acsabm.0c01136.
[30] M. Serata, T. Iino, E. Yasuda, T. Sako, Roles of thioredoxin and thioredoxin reductase in the resistance to oxidative stress in *Lactobacillus casei*, Microbiology (Reading) 158 (Pt 4) (2012) 953–962, https://doi.org/10.1099/MIC.0.053942-0.
[31] H. Kinoshita, H. Uchida, Y. Kawai, T. Kawasaki, N. Wakahara, H. Matsuo, M. Watanabe, H. Kitazawa, S. Ohnuma, K. Miura, A. Horii, T. Saito, Cell surface *Lactobacillus plantarum* LA 318 glyceraldehyde-3-phosphate dehydrogenase (GAPDH) adheres to human colonic mucin, J. Appl. Microbiol. 104 (6) (2008) 1667–1674, https://doi.org/10.1111/J.1365-2672.2007.03679.X.
[32] P. Briaud, R.K. Carroll, Extracellular vesicle biogenesis and functions in gram-positive bacteria, Infect. Immun. 88 (12) (2020), https://doi.org/10.1128/IAI.00433-20.
[33] T. Smyth, K. Petrova, N.M. Payton, I. Persaud, J.S. Redzic, M.W. Graner, P. Smith-Jones, T.J. Anchordoquy, Surface functionalization of exosomes using click chemistry, Bioconjug. Chem. 25 (10) (2014) 1777–1784, https://doi.org/10.1021/BC500291R.
[34] K.M. Brothers, N.A. Stella, K.M. Hunt, E.G. Romanowski, X. Liu, J.K. Klarlund, R.M. Q. Shanks, Putting on the brakes: bacterial impediment of wound healing, Sci. Rep. 5 (1) (2015) 1–14, https://doi.org/10.1038/srep14003.
[35] P. Torres, M. Castro, M. Reyes, V.A. Torres, Histatins, wound healing, and cell migration, Oral Dis. 24 (7) (2018) 1150–1160, https://doi.org/10.1111/ODI.12816.
[36] A. Oryan, E. Alemzadeh, M.H. Eskandari, Kefir accelerates burn wound healing through inducing fibroblast cell migration in vitro and modulating the expression of IL-1ß, TGF-SS1, and BFGF genes in vivo, Probiotics Antimicrob. Proteins 11 (3) (2019) 874–886, https://doi.org/10.1007/S12602-018-9435-6.
[37] G.A. Preidis, D.M. Saulnier, S.E. Blutt, T.-A. Mistretta, K.P. Riehle, A.M. Major, S. F. Venable, M.J. Finegold, J.F. Petrosino, M.E. Conner, J. Versalovic, Probiotics stimulate enterocyte migration and microbial diversity in the neonatal mouse intestine, FASEB J. 26 (5) (2012) 1960, https://doi.org/10.1096/FJ.10-177980.
[38] M. Peura, J. Bizik, P. Salmenperä, A. Noro, M. Korhonen, T. Pätilä, A. Vento, A. Vaheri, R. Alitalo, J. Vuola, A. Harjula, E. Kankuri, Bone marrow mesenchymal stem cells undergo nemosis and induce keratinocyte wound healing utilizing the HGF/c-met/PI3K pathway, Wound Repair Regen. 17 (4) (2009) 569–577, https://doi.org/10.1111/J.1524-475X.2009.00507.X.
[39] S. Cheng, Z. Xi, G. Chen, K. Liu, R. Ma, C. Zhou, Extracellular vesicle-carried MicroRNA-27b derived from mesenchymal stem cells accelerates cutaneous wound healing via E3 ubiquitin ligase ITCH, J. Cell. Mol. Med. 24 (19) (2020) 11254–11271, https://doi.org/10.1111/JCMM.15692.
[40] T.A. Wynn, Type 2 cytokines: mechanisms and therapeutic strategies, Nat. Rev. Immunol. 15 (5) (2015) 271–282, https://doi.org/10.1038/nri3831.
[41] A. Tsurumi, Y.A. Que, C.M. Ryan, R.G. Tompkins, L.G. Rahme, TNF-α/IL-10 ratio correlates with burn severity and may serve as a risk predictor of increased susceptibility to infections, Front. Public Health 4 (OCT) (2016) 216, https://doi.org/10.3389/FPUBH.2016.00216/PDF.
[42] M.K. Perera, N.P. Herath, S.L. Pathirana, M. Phone-Kyaw, H.K. Alles, K.N. Mendis, S. Premawansa, S.M. Handunnetti, Association of high plasma TNF-alpha levels and TNF-alpha/IL-10 ratios with TNF2 allele in severe *P. falciparum* malaria patients in Sri Lanka, Pathog. Glob. Health 107 (1) (2013) 21–29, https://doi.org/10.1179/2047773212Y.
[43] B. Goswami, M. Rajappa, V. Mallika, D.K. Shukla, S. Kumar, TNF-alpha/IL-10 ratio and C-reactive protein as markers of the inflammatory response in CAD-prone north Indian patients with acute myocardial infarction, Clin. Chim. Acta 408 (1–2) (2009) 14–18, https://doi.org/10.1016/J.CCA.2009.06.029.
[44] M. Mata Forsberg, S. Björkander, Y. Pang, L. Lundqvist, M. Ndi, M. Ott, I.B. Escribá, M.C. Jaeger, S. Roos, E. Sverremark-Ekström, Extracellular membrane vesicles from lactobacilli dampen IFN-γ responses in a monocyte-dependent manner, Sci. Rep. 9 (1) (2019) 17109, https://doi.org/10.1038/s41598-019-53576-6.
[45] J.S. Ong, T.D. Taylor, C.C. Yong, B.Y. Khoo, S. Sasidharan, S.B. Choi, H. Ohno, M. T. Liong, *Lactobacillus plantarum* USM8613 aids in wound healing and suppresses staphylococcus aureus infection at wound sites, Probiotics Antimicrob. Proteins 12 (1) (2020) 125–137, https://doi.org/10.1007/S12602-018-9505-9.
[46] A. Grada, J. Mervis, V. Falanga, Research techniques made simple: animal models of wound healing, J. Investig. Dermatol. 138 (10) (2018) 2095–2105.e1, https://doi.org/10.1016/J.JID.2018.08.005.
[47] V. Falanga, D. Schrayer, J. Cha, J. Butmarc, P. Carson, A.B. Roberts, S.J. Kim, Full-thickness wounding of the mouse tail as a model for delayed wound healing: accelerated wound closure in Smad3 Knock-out mice, Wound Repair Regen. 12 (3) (2004) 320–326, https://doi.org/10.1111/J.1067-1927.2004.012316.X.
[48] P.A. Gerber, B.A. Buhren, H. Schrumpf, B. Homey, A. Zlotnik, P. Hevezi, The top skin-associated genes: a comparative analysis of human and mouse skin transcriptomes, Biol. Chem. 395 (6) (2014) 577–591, https://doi.org/10.1515/HSZ-2013-0279/DOWNLOADASSET/SUPPL/20130279GERBER_ET_AL-BIOL_CHEM-SKINGENES_-_SUPPLEMENTS.DOC.
[49] A.L. Rippa, E.P. Kalabusheva, E.A. Vorotelyak, Regeneration of dermis: scarring and cells involved, Cells 8 (6) (2019) 607, https://doi.org/10.3390/CELLS8060607.
[50] H. Il Kim, C.Y. Kwak, H.Y. Kim, H.S. Yi, E.J. Park, J.H. Kim, J.H. Park, Correlation between dermal thickness and scar formation in female patients after thyroidectomy, Arch. Craniofac. Surg. 19 (2) (2018) 120, https://doi.org/10.7181/ACFS.2018.01907.
[51] C. Brochhausen, V.H. Schmitt, A. Mamilos, C. Schmitt, C.N.E. Planck, T.K. Rajab, H. Hierlemann, C.J. Kirkpatrick, Expression of CD68 positive macrophages in the use of different barrier materials to prevent peritoneal adhesions—an animal study, J. Mater. Sci. Mater. Med. 28 (1) (2017) 1–15, https://doi.org/10.1007/S10856-016-5821-3.
[52] E. Vågesjö, E. Öhnstedt, A. Mortier, H. Lofton, F. Huss, P. Proost, S. Roos, M. Phillipson, Accelerated wound healing in mice by on-site production and delivery of CXCL12 by transformed lactic acid Bacteria, Proc. Natl. Acad. Sci. U. S. A. 115 (8) (2018) 1895–1900, https://doi.org/10.1073/PNAS.1716580115/-/DCSUPPLEMENTAL.
[53] W. Mohammedsaeed, S. Cruickshank, A.J. McBain, C.A. O'Neill, *Lactobacillus Rhamnosus* GG Lysate increases re-epithelialization of keratinocyte scratch assays by promoting migration, Sci. Rep. 5 (1) (2015) 1–11, https://doi.org/10.1038/srep16147.
[54] A. Aljohmani, B. Opitz, M. Bischoff, D. Yildiz, *Pseudomonas aeruginosa* triggered exosomal release of ADAM10 mediates proteolytic cleavage in trans, Int. J. Mol. Sci. 23 (3) (2022), https://doi.org/10.3390/IJMS23031259.
[55] T.A. Wilgus, S. Roy, J.C. McDaniel, Neutrophils and wound repair: positive actions and negative reactions, Adv. Wound Care (New Rochelle) 2 (7) (2013) 379–388, https://doi.org/10.1089/wound.2012.0383.